

Quantification of interfacial spin-charge conversion in metal/insulator hybrid structures by generalized boundary conditions

Cristina Sanz-Fernández,^{*,†,⊥} Van Tuong Pham,^{*,†,⊥} Edurne Sagasta,[‡] Luis E. Hueso,[‡] Ilya V. Tokatly,^{*,§} Fèlix Casanova,^{*,‡} and F. Sebastián Bergeret^{*,†}

[†]*Centro de Física de Materiales (CFM-MPC), Centro Mixto CSIC-UPV/EHU, 20018 Donostia-San Sebastián, Basque Country, Spain*

[‡]*CIC nanoGUNE, 20018 Donostia-San Sebastián, Basque Country, Spain*

[¶]*IKERBASQUE, Basque Foundation for Science, 48013 Bilbao, Basque Country, Spain*

[§]*Nano-Bio Spectroscopy Group, Departamento de Física de Materiales, Universidad del País Vasco (UPV/EHU), 20018 Donostia-San Sebastián, Basque Country, Spain*

^{||}*Donostia International Physics Center (DIPC), 20018 Donostia-San Sebastián, Basque Country, Spain*

[⊥]*Contributed equally to this work*

E-mail: cristina_sanz001@ehu.eus; v.pham@nanogune.eu; ilya.tokatly@ehu.es;

f.casanova@nanogune.eu; fs.bergeret@csic.es

Abstract

We present and verify experimentally a universal theoretical framework for the description of spin-charge interconversion in non-magnetic metal/insulator structures with interfacial spin-orbit coupling (ISOC). Our formulation is based on drift-diffusion equations supplemented with generalized boundary conditions. The latter encode the

effects of ISOC and relate the electronic transport in such systems to spin loss and spin-charge interconversion at the interface, which are parameterized, respectively, by $G_{\parallel/\perp}$ and $\sigma_{sc/cs}$. We demonstrate that the conversion efficiency depends solely on these interfacial parameters. We apply our formalism to two typical spintronic devices that exploit ISOC: a lateral spin valve and a multilayer Hall bar, for which we calculate the non-local resistance and the spin Hall magnetoresistance, respectively. Finally, we perform measurements on these two devices with a BiO_x/Cu interface and verify that transport properties related to the ISOC are quantified by the same set of interfacial parameters.

A thorough understanding of charge and spin transport is crucial for the development of devices based on the electric control of spin currents.^{1,2} In this respect, the charge-spin interconversion via spin-orbit coupling (SOC) plays a key role. SOC leads to the widely studied spin Hall (SHE)³⁻⁵ and Edelstein (EE) effects,⁶⁻⁹ which are at the basis of spin-orbit torque memories¹⁰⁻¹² and spin-based logic devices.^{13,14}

Of particular interest are systems with sizable spin-charge interconversion at the interface between an insulator (I) that contains a heavy element, and a normal metal (N) with negligible SOC and long spin relaxation length, as for example BiO_x/Cu bilayers. In these systems, the spin-charge interconversion occurs at the hybrid interface via an interfacial spin-orbit coupling (ISOC).^{15,16} Whereas the electronic transport in N is well described by customary drift-diffusion equations, the interfacial effects occur at atomic scales near the interface and, hence, their inclusion into the drift-diffusion model is kind of subtle. Some works use an intuitive picture based on the idealized two-dimensional Rashba model and assume the existence of a two-dimensional electron gas with Rashba SOC at the interface,¹⁶⁻¹⁸ in which the conversion takes place via the EE and its inverse (IEE). Such description is clearly valid for conductive surface states in (e.g. topological) insulators^{19,20} or two-dimensional electron gases.^{21,22} However, in metallic systems, it requires the introduction of additional microscopic parameters to model the coupling between interface states and the diffusive motion

of electrons in the metal. Moreover, the very existence of a well-defined two-dimensional interface band, and its relevance for the electronic transport, in systems like BiO_x/Cu is not obvious as realistic device structures are frequently polycrystalline and quite disordered. Apparently, the physical picture involving the interface band with Rashba SOC is merely one of the possible interpretations for the experimental data. One can contemplate other microscopic scenarios to describe the charge-spin coupling in I/N systems. For example, in the BiO_x/Cu interface, one could assume that Bi atoms diffuse into Cu and induce an effective “extrinsic” SOC in a thin layer near the interface. Alternatively, a spin-charge interconversion can be generated via an interfacial spin-dependent scattering of the bulk Bloch states (see, for example, Refs. [23–25](#)). Each of these models will provide a different set of microscopic parameters, which usually have to be inferred from the measurements of macroscopic transport properties.

In this Letter, we approach the problem from a different angle and propose a universal theoretical framework which is independent of microscopic mechanisms and details. Specifically, we provide the basic drift-diffusion theory describing the charge and spin transport in I/N structures. To account for the ISOC, we use the effective boundary conditions (BCs) derived in Ref. [26](#). In this work, such BCs basically describe two types of interfacial processes mediated by ISOC: spin-charge interconversion and spin losses, quantified respectively by the interfacial spin-to-charge/charge-to-spin conductivities, $\sigma_{sc/cs}$, and the spin loss conductances $G_{\parallel/\perp}$ for spins polarized parallel/perpendicular to the interface. The efficiency of spin-charge interconversion, which is central to the development of spintronic devices, is determined by the ratio between the strengths of these two processes. This ratio coincides with the widely used conversion efficiency, the inverse Edelstein length λ_{IEE} , such that $\lambda_{\text{IEE}} = \sigma_{sc}/G_{\parallel}$. We apply our theory to describe two typical experimental setups: a lateral spin valve (LSV) made of Cu wires with a middle wire partially covered by a BiO_x layer (see Fig. [2a](#)), where non-local resistances are measured, and a $\text{BiO}_x/\text{Cu}/\text{YIG}$ trilayer Hall bar (see Fig. [4a](#)), where we measure the spin Hall magnetoresistance (SMR). From contrasting

the experimental results with our theory, we demonstrate that $\sigma_{\text{sc}} = \sigma_{\text{cs}}$, which confirms the Onsager reciprocity. In addition, both experiments can be described by similar values of the ISOC parameters when measured at the same temperature. This confirms that the spin-charge interconversion in those systems only depends on the intrinsic properties of the BiO_x/Cu interface.

Model and method

We consider a customary setup consisting of a normal metal (N) with negligible spin-orbit coupling adjacent to a non-magnetic insulator (I), see Fig. 1. In the N layer, spin and charge transport is described by the diffusion equations:

$$\nabla^2 \hat{\mu} = \frac{\hat{\mu}}{\lambda_{\text{N}}^2}, \quad (1)$$

$$\nabla^2 \mu = 0. \quad (2)$$

Here, $\hat{\mu} = (\mu^x, \mu^y, \mu^z)$ and μ are the spin and charge electrochemical potentials (ECP), where hat symbol indicates spin pseudovector. It is assumed that N has inversion symmetry and the spin relaxation is isotropic and described by the bulk spin diffusion length λ_{N} .²⁷ The diffusive charge and spin currents are defined as $e\hat{\mathbf{j}} = -\sigma_{\text{N}}\nabla\hat{\mu}$ and $e\mathbf{j} = -\sigma_{\text{N}}\nabla\mu$, respectively, with $e = -|e|$.

Equations (1) and (2) are complemented by boundary conditions (BCs) at the interfaces. Specifically, at the interface with vacuum, one imposes a zero current condition. Whereas, at the I/N interface with ISOC, the BCs read:²⁶

$$-\sigma_{\text{N}}(\nabla \cdot \mathbf{n})\hat{\mu}|_0 = G_{\perp} \hat{\mu}_{\perp}|_0 + G_{\parallel} \hat{\mu}_{\parallel}|_0 + \sigma_{\text{cs}} (\mathbf{n} \times \nabla) \mu|_0, \quad (3)$$

$$-\sigma_N(\nabla \cdot \mathbf{n})\mu|_0 = \sigma_{sc}(\mathbf{n} \times \nabla)\hat{\mu}|_0. \quad (4)$$

We denote by \mathbf{n} the vector normal to the interface, pointing from the metal towards the interface, and σ_N is the conductivity of N. Equation (3) is the BC for the spin ECP. The last term in the r.h.s. describes the charge-to-spin conversion, whose efficiency is described by the conductivity σ_{cs} . As schematically shown in Fig. 1a, this term couples an effective electric field and the spin current density at the interface,^{26,28–30} and can be interpreted as an interfacial spin Hall conductivity. Alternatively, it can be interpreted as if the charge current induces an homogeneous spin ECP via an interfacial Edelstein effect (EE), which in turn diffuses into the bulk conductor. These two interpretations are fully compatible within the present formalism. The second type of processes which take place at the interface are spin losses (first two terms in the r.h.s. of Eq. (3)), which are quantified by the corresponding spin loss conductance density per area $G_{\perp/\parallel}$ for spins perpendicular/parallel ($\hat{\mu}_{\perp}/\hat{\mu}_{\parallel}$) to the interface.

Equation (4) is the BC for the charge ECP. The charge is obviously conserved and, therefore, the r.h.s. only contains the spin-to-charge conversion between a diffusive bulk spin current and an interfacial charge current, which induces a voltage drop. The last term in Eqs. (3) and (4) describes reciprocal effects.¹ Equation (4) can be interpreted as an interfacial inverse spin Hall effect (ISHE), which couples the charge and the spin currents. But again, an alternative interpretation is possible: from the conservation of the charge current at the interface, we can relate the bulk charge current to the divergence of an interfacial current as $\sigma_N(\nabla \cdot \mathbf{n})\mu|_0 = -e\nabla \cdot \mathbf{j}_I$. Comparing this last equation with Eq. (4),

¹Symmetry arguments alone cannot fix the relation between σ_{sc} and σ_{cs} .²⁶ However, we will see by contrasting theory with experiment, that reciprocity requires $\sigma_{sc} = \sigma_{cs}$.

we may define the interfacial charge current density as:²

$$e\mathbf{j}_I = -\sigma_{sc} (\mathbf{n} \times \hat{\mu}) \Big|_0. \quad (5)$$

Written this way, BC (4) describes the conversion of a non-equilibrium spin into an interfacial charge current, which corresponds to what is usually called the interfacial inverse Edelstein effect (IEE), as illustrated in Fig. 1b.

Within this last interpretation, we can introduce the commonly used conversion parameter λ_{IEE} . It has dimensions of a length and is defined as the ratio between the amplitude of the induced interfacial charge current density, \mathbf{j}_I , and the amplitude of the spin current injected to the interface from the bulk, $\sigma_N(\nabla \cdot \mathbf{n})\hat{\mu}|_0$. From Eq. (5), one can see that the effect is finite only if the spin current is polarized in a direction parallel to the interface. By using Eqs. (3) and (5), we then obtain:

$$\lambda_{IEE} = \frac{\sigma_{sc}}{G_{\parallel}}. \quad (6)$$

This is a remarkable result that follows straightforwardly from our description. λ_{IEE} is purely determined by interfacial parameters and it is indeed a quantification of the conversion efficiency since it is the ratio between the spin-to-charge conversion and the spin loss at the interface. Note that both parameters, σ_{sc} and G_{\parallel} , are finite only in the presence of a finite ISOC. Their specific values depend on the microscopic properties of the interface, which are intrinsic for each material combination. Both σ_{sc} and G_{\parallel} may depend on temperature and, thus, λ_{IEE} is also temperature dependent.

From an experimental perspective, the spin-to-charge conversion is usually detected electrically, by measuring a voltage drop. Typical devices are shown in Figs. 2a and 4a, where

²Notice that, in principle, an additional divergenceless term may appear in the r.h.s. of Eq. (5). Indeed, as demonstrated in Ref. 26, symmetry allows for a term proportional to the out-of-plane component of the spin ECP. In the present work, we only consider spin polarization parallel to the I/N interface and, hence, we neglect that term.

transverse voltages are measured. In theory, one needs to determine and integrate the charge ECP to determine the averaged voltage drop between two points. For concreteness, we consider the generic setup shown in Fig. 1b, in which a spin current polarized in the x direction flows towards the interface, such that a voltage difference is generated in the transverse, y , direction according to Eq. (5). The averaged voltage drop is measured between the points $y = \pm L_y/2$, with L_y the total length in the y direction, and is given by (see Note S1 for details):

$$V_{\text{sc}} = \frac{\sigma_{\text{sc}}}{e\sigma_{\text{N}}A_{\text{N}}} \iint_{-\frac{L_y}{2}}^{\frac{L_y}{2}} (\mathbf{n} \times \hat{\mu}|_0) \cdot \mathbf{e}_y \, dx dy , \quad (7)$$

where $A_{\text{N}} = t_{\text{N}}w_{\text{N}}$ is the cross-sectional area of the wire, with t_{N} and w_{N} being its thickness and width, respectively, over which the voltage drop is averaged. Equation (7) shows that the voltage drop between two points is proportional to the total spin accumulation created via the ISOC between them.

In the following, we apply the above formalism to derive the voltage drop associated to spin-charge interconversions in two different devices.

Results and discussion

We start analyzing the double LSV shown in Fig. 2a (see Note S2 for fabrication and measurement details). A charge current I_c is injected from the Permalloy (Py) injector F2 into a Cu wire. F2 forms a LSV either with the detector F1 or F3. We use the LSV between F2 and F1 as a reference setup. In the LSV between F2 and F3 there is an additional transverse Cu wire covered by a BiO_x layer (red in Fig. 2a) and, hence, ISOC at the BiO_x/Cu interface. In this case, part of the spin current in the main Cu wire is absorbed and converted to a transverse charge current (see Fig. 1b).

Quantitative description of the spin injection, diffusion, and detection in LSVs has been widely studied in the literature.^{31,32} In our setup, the thickness t_{N} and width w_{N} of the Cu wires are much smaller than the spin diffusion length λ_{N} , and one can integrate the

spin diffusion equation (1) over the wire cross-section and simplify it to a one-dimensional problem,^{31–33} as sketched in Fig. 2b. At the BiO_x/Cu middle wire, the z -integration using the BC at $z = 0$ of Eq. (3), leads to a renormalization of λ_N (see Note S3):

$$\lambda_{N\parallel} = \frac{\lambda_N}{\sqrt{1 + \frac{G_{\parallel}\lambda_N^2}{\sigma_N t_N}}}, \quad (8)$$

where we neglect corrections of order σ_{sc}^2 .

At the crossing point, $x = 0$ in Fig. 2b, we use Kirchhoff's law for the spin currents (see Note S3):

$$-A_N\sigma_N\partial_x\hat{\mu}_{\parallel}\Big|_{0^-}^{0^+} = -G_{N\parallel}\hat{\mu}_{\parallel}\Big|_{x=0} - A_n^{\text{eff}}\sigma_{cs}\frac{ej_c}{\sigma_N}\hat{\mathbf{e}}_x. \quad (9)$$

Here, $G_{N\parallel} = \frac{t_N\sigma_N A_n^{\text{eff}}}{\lambda_{N\parallel}^2}$ is the effective spin (bulk) conductance of the BiO_x/Cu wire, with $A_n^{\text{eff}} = w_N(w_N + 2\lambda_{N\parallel})$. The latter is the effective area of the BiO_x/Cu interface that absorbs (injects) spin current. Indeed, the r.h.s. of this equation corresponds to Eq. (3) with an effective spin loss conductance counting for both the interfacial and bulk spin losses at the middle wire. The last term in Eq. (9) corresponds to the last term in Eq. (3) and it is proportional to the total injected charge current I_c along the middle wire oriented in the y direction. If we assume an homogeneous distribution of the current, then $\mathbf{j}_c = \frac{I_c}{A_N}\hat{\mathbf{e}}_y$.

The Cu/Py interfaces are described by the following BC:^{31,34,35}

$$\begin{aligned} -A_N\sigma_N\partial_x\hat{\mu}_{\parallel}\Big|_{x=-\frac{L_x^+}{2}}^{x=-\frac{L_x^-}{2}} &= -A_F\left(\sigma_F^*\partial_y\hat{\mu}_{\parallel F2}\Big|_{y=0} + p_F ej_c\right), \\ -A_N\sigma_N\partial_x\hat{\mu}_{\parallel}\Big|_{x=\frac{L_x^-}{2}}^{x=\frac{L_x^+}{2}} &= -A_F\sigma_F^*\partial_y\hat{\mu}_{\parallel F3}\Big|_{y=0}, \end{aligned} \quad (10)$$

where $\hat{\mu}_{\parallel F2}$ and $\hat{\mu}_{\parallel F3}$ are the spin ECPs at ferromagnets F2 and F3, respectively. The polarization and effective conductivity at the ferromagnets are p_F and $\sigma_F^* = \sigma_F(1 - p_F^2)$, respectively, and L_x is the distance between consecutive ferromagnetic wires. Since the spin current strongly decreases at the ferromagnets, A_F corresponds to the Py/Cu junction area.³¹ The last term of the first equation above is proportional to the charge current density,

$j_c = \frac{I_c}{A_F}$, (homogeneously) injected at the ferromagnetic wire. For the description of the reference LSV, we substitute F3 by F1 in the second BC. Because the Py/Cu interfaces are good metallic contacts we assume the continuity of $\hat{\mu}_{\parallel}$. This condition, together with the one-dimensional version of Eq. (1) and the BCs (9) and (10), determine the full spatial dependence of $\hat{\mu}_{\parallel}$.

We are interested in the value of $\hat{\mu}_{\parallel}$ at the detectors F1/F3 which is proportional to the non-local voltages $V_{\text{nl}} = e^{-1} p_F \hat{\mu}_{\parallel|F1/F3}|_{y=0}$ ^{31,36} (see Fig. 2b). From such non-local measurement, we determine the non-local resistance, $R_{\text{nl}} = V_{\text{nl}}/I_c$, where I_c is the current injected from F2. The value of R_{nl} changes sign when the magnetic configuration of injector and detector ferromagnets changes from parallel, R_{nl}^{P} , to antiparallel, $R_{\text{nl}}^{\text{AP}}$, which experimentally allows us to remove any baseline resistance coming from non-spin related effects by taking $\Delta R_{\text{nl}} = R_{\text{nl}}^{\text{P}} - R_{\text{nl}}^{\text{AP}}$ (see Fig. 3a). Comparing the non-local resistance measured at F3, $\Delta R_{\text{nl}}^{\text{abs}}$, with the one measured at F1 at the reference LSV, $\Delta R_{\text{nl}}^{\text{ref}}$, the magnitude of the spin absorption^{32,37} and, therefore, the value of the spin loss conductance, G_{\parallel} , can be obtained from our model. For this, we compute the ratio $\Delta R_{\text{nl}}^{\text{abs.}}/\Delta R_{\text{nl}}^{\text{ref.}} = \hat{\mu}_{\parallel|F3}/\hat{\mu}_{\parallel|F1}|_{y=0}$ by solving the full boundary problem and obtain the following expression:

$$\frac{\Delta R_{\text{nl}}^{\text{abs.}}}{\Delta R_{\text{nl}}^{\text{ref.}}} = \left[1 + \frac{G_{\text{N}\parallel} (G_{\text{F}} + 2G_{\text{N}}) - G_{\text{F}} e^{-\frac{L_x}{\lambda_{\text{N}}}}}{2G_{\text{N}} (G_{\text{F}} + 2G_{\text{N}}) + G_{\text{F}} e^{-\frac{L_x}{\lambda_{\text{N}}}}} \right]^{-1}. \quad (11)$$

Here, $G_i = \frac{\sigma_i A_i}{\lambda_i}$ are the spin conductances of the Cu and Py wires, with λ_i , σ_i , and A_i , the corresponding parameters for the bare Cu wire ($i = \text{N}$) and the ferromagnet ($i = \text{F}$). The form of Eq. (11) agrees with the one obtained in previous works.³⁷ However, our formulation is more general since it distinguishes via $G_{\text{N}\parallel}$ between interfacial and bulk losses at the BiO_x/Cu wire. Consequently, we can ensure that our calculation of the ISOC parameter G_{\parallel} and, therefore, λ_{IEE} , is only related to interfacial effects (see Eqs. (6), (8), and (9)).

Interestingly, Fig. 3b shows weak temperature dependence of the absorption ratio, $\Delta R_{\text{nl}}^{\text{abs.}}/\Delta R_{\text{nl}}^{\text{ref.}} \approx 0.5$, revealing that about half of the spin current is absorbed at the BiO_x/Cu middle wire.

For the calculation of G_{\parallel} via Eq. (11), the resistivity of the Cu layer is carefully measured as a function of the temperature (see Note S4), with $t_N = w_N = 80$ nm, and $L_x = 570$ nm. Assuming that the magnetic properties of Py and the specific spin resistivities of Py and Cu of our device are the same as in Ref. 38, we use the same temperature dependence of ρ_F and p_F , and the constant spin resistivities $\lambda_F/\sigma_F = 0.91$ f Ωm^2 and $\lambda_N/\sigma_N = 18.3$ f Ωm^2 . By inserting these experimental values in Eq. (11) for different temperatures, we obtain the temperature dependence of the spin loss conductance G_{\parallel} for the BiO_x/Cu interface shown in Fig. 3b. A slight decrease of G_{\parallel} can be observed with increasing temperature, which seems to arise from the Cu conductivity. A linear relation between G_{\parallel} and σ_N (see Note S5A) suggests a Dyakonov-Perel mechanism of the spin loss, expected for a Rashba interface, which also agrees with the observations of Ref. 39.

In addition, we can determine $\sigma_{sc/cs}$ in the same device. By injecting a charge current I_c from F2, a x -polarized spin current is created and reaches the BiO_x/Cu wire, where a conversion to a transverse charge current occurs via Eq. (5). This is detected as a non-local voltage V_{sc} along the BiO_x/Cu wire and the non-local resistance $R_{sc}^{LSV} = V_{sc}/I_c$ is determined as a function of an in-plane magnetic field along the hard axis of F2, B_x . By reversing the orientation of the magnetic field, the opposite R_{sc}^{LSV} is obtained, since the Py magnetization is reversed as well as the orientation of the spin polarization (see Fig. 3c). The difference of the two values for R_{sc}^{LSV} , denoted as $2\Delta R_{sc}^{LSV}$ in Fig. 3c, allows to remove any baseline resistance. By swapping the voltage and current probes, the reciprocal charge-to-spin conversion signal, $R_{cs}^{LSV} = V_{cs}/I_c$, can also be measured.

Theoretically, from the calculation of the spatial dependence of the spin ECP, we compute both V_{sc} , from Eq. (7), and $V_{cs} = e^{-1}p_F\mu_{\parallel F2}^x|_{y=0}$, by assuming a homogeneous spin absorption/injection at A_n^{eff} . We obtain the same expressions, with opposite sign:

$$\Delta R_{sc/cs}^{LSV} = \pm \frac{\sigma_{sc/cs}}{\sigma_N} \frac{A_n^{\text{eff}}}{A_N} \frac{p_F e^{\frac{L_x}{2\lambda_N}}}{G_F \left(1 - \frac{G_{N\parallel}}{2G_N}\right) + e^{\frac{L_x}{\lambda_N}} (G_F + 2G_N) \left(1 + \frac{G_{N\parallel}}{2G_N}\right)}. \quad (12)$$

Experimentally, Figs. 3c and 3d confirm the reciprocity between both measurements, $\Delta R_{cs}^{\text{LSV}} = \Delta R_{sc}^{\text{LSV}}$. The broken time reversal symmetry, due to the magnetic contacts, leads to the opposite sign for reciprocal measurements. By contrasting this with the result of Eq. (12), one confirms that $\sigma_{sc} = \sigma_{cs}$. The experimental value for $2\Delta R_{sc}^{\text{LSV}} \approx 15 \pm 3\mu\Omega$ at 10 K yields $\sigma_{sc/cs} \approx 44 \pm 9 \Omega^{-1} \text{cm}^{-1}$ for the spin-charge conductivity and $\lambda_{\text{IEE}} \approx 0.16 \pm 0.03 \text{ nm}$. This value is of same order of magnitude, but somewhat smaller, than previous reported results obtained by spin pumping experiments, $\lambda_{\text{IEE}} \approx 0.2 - 0.7 \text{ nm}$,^{15,18,39} and LSV experiments, $\lambda_{\text{IEE}} \approx 0.5 - 1 \text{ nm}$.³³ This discrepancy might be due to a different quality of the BiO_x/Cu interface: *ex-situ* deposition in this experiment (see Note S2) and *in-situ* deposition in the other works. The temperature dependence of the different parameters is presented in Note S5B. One observes a decreasing trend of σ_{sc} by increasing the temperature, which translates in a decreasing of the Edelstein length, in agreement with previous literature.³⁹

In order to check the accuracy of our 1D model, we have performed a 3D finite element method simulation detailed in Note S6. Figure 2c shows the geometry of the simulated device and the mesh of the finite elements. The interface with ISOC is simulated as a thin layer with finite thickness t_{int} and characterized by a spin diffusion length λ_{int} and an effective spin Hall angle $\theta_{\text{int}}^{\text{eff}}$. Using the definition of the Edelstein length as $\frac{1}{2}\theta_{\text{int}}^{\text{eff}}t_{\text{int}}$,⁴⁰ we obtain $\lambda_{\text{IEE}} = 0.10 \pm 0.02 \text{ nm}$, in good agreement with the λ_{IEE} estimated from our 1D model.

In order to verify that both ISOC parameters, G_{\parallel} and σ_{sc} , are interface specific, we carry out an additional experiment involving a BiO_x/Cu interface. Namely, we measure the SMR in a Cu layer sandwiched between a BiO_x (at $z = 0$) and a YIG layers (at $z = -t_N$), shaped as a Hall bar, as shown in Fig. 4a (see Note S2 for fabrication and measurement details). In this setup, see Fig. 4b, a charge current I_c in the longitudinal direction (x direction), induces an out-of-plane spin current density via the ISOC, described by the last term of Eq. (3). This spin current, polarized in the y direction, propagates towards the Cu/YIG interface where is partly reflected and modified.⁴¹⁻⁴³ The reflected spin current diffuses back to the BiO_x/Cu interface, where it is converted back to an interfacial charge current via the reciprocal effect.

Therefore, the overall effect is of second order in ISOC and proportional to $\sigma_{\text{cs}}\sigma_{\text{sc}} = \sigma_{\text{sc}}^2$.

YIG is an insulating ferrimagnetic material and the electron spin reflection at the Cu/YIG interface depends on the direction of magnetization of the YIG, denoted as \mathbf{m} . The effective BC describing this interface is well-known and reads as follows:^{44 3}

$$-\sigma_{\text{N}}(\nabla \cdot \mathbf{n})\hat{\mu}|_{-t_{\text{N}}} = G_{\text{s}} \hat{\mu}|_{-t_{\text{N}}} + G_{\text{r}} \mathbf{m} \times (\hat{\mu} \times \mathbf{m})|_{-t_{\text{N}}} + G_{\text{i}} (\mathbf{m} \times \hat{\mu})|_{-t_{\text{N}}}. \quad (13)$$

Here, $G_{\text{r,i}}$ are the real and imaginary parts of the spin-mixing conductance (per area), $G_{\uparrow\downarrow} = G_{\text{r}} + iG_{\text{i}}$, and G_{s} is the so-called spin-sink conductance. The values of these parameters are known for YIG, where $G_{\text{i}} \ll G_{\text{s}} < G_{\text{r}}$ and, hence, G_{i} can be neglected.^{43,45–47}

In the experiment, the transverse angular dependent magnetoresistance (TADMR) measurement is performed in the Hall bar of BiO_x/Cu grown on a YIG substrate as shown in Fig. 4a. The transverse voltage depends on the direction of the in-plane applied magnetic field, parameterized by the angle α . The experimental results for the TADMR, $R_{\text{T}} = V_{\text{T}}/I_{\text{c}}$, are shown in Fig. 4c.

To calculate R_{T} , we first determine the spatial dependence of the spin ECP from Eq. (1) and BCs Eq. (3) and Eq. (13) at the BiO_x/Cu and Cu/YIG interfaces, respectively. We assume that the system is translational invariant in the x - y plane and reduce the diffusion problem to a 1D problem in the z direction. We then use Eq. (7) to obtain V_{T} , averaged in the cross-sectional area A_{N} . This results in:

$$R_{\text{T}} \approx \frac{\sigma_{\text{sc}}^2}{2\sigma_{\text{N}}^2 t_{\text{N}}^2} \frac{G_{\text{r}}}{(G_{\parallel} + G_{\text{s}})(G_{\parallel} + G_{\text{s}} + G_{\text{r}})} \sin(2\alpha) = \Delta R_{\text{T}} \sin(2\alpha). \quad (14)$$

We denote by ΔR_{T} the amplitude of the modulation and assume that $\lambda_{\text{N}} \gg t_{\text{N}}$ (see Note S7 for the exact expression). Note that the parameters of the Cu/YIG interface, $G_{\text{r,s}}$, add to the spin loss at the BiO_x/Cu interface G_{\parallel} . We identify by comparison of Eqs. (3) and (13)

³Following our convention the vector \mathbf{n} normal to the interface, points from the Cu towards the insulating layer.

two effective spin loss conductances, $G_x = (G_{\parallel} + G_s)$ and $G_y = (G_{\parallel} + G_s + G_r)$, for spins polarized in the x and y directions, respectively. The amplitude of the SMR signal is then, according to Eq. (14), proportional to the difference $G_x - G_y$.

From Figure 4c, we estimate $\Delta R_T \approx 0.03 \text{ m}\Omega$ at $T = 130 \text{ K}$. At this temperature, from the LSV measurements, we obtain for the BiO_x/Cu ISOC parameters $G_{\parallel} \approx 1.5 \times 10^{13} \Omega^{-1} \text{ m}^{-2}$ and $\sigma_{sc/cs} \approx 11.3 \Omega^{-1} \text{ cm}^{-1}$, as shown in Figs. 3b and S3b, respectively. The spin conductances G_s and G_r in light metal/YIG interfaces have been estimated in evaporated Cu and Al.^{48,49} Whereas $G_s = 3.6 \times 10^{12} \Omega^{-1} \text{ m}^{-2}$ for Cu/YIG⁴⁹ is a consistent value in the literature,^{48,50} the reported G_r is very low,⁴⁹ as generally observed in evaporated metals on YIG.^{48,51} By substituting G_{\parallel} , G_s , and $\sigma_{sc/cs}$ values in Eq. (14), we obtain $G_r \approx 6.1 \times 10^{13} \Omega^{-1} \text{ m}^{-2}$. This value for sputtered Cu on YIG is much larger than that estimated in evaporated Cu on YIG, in agreement with the reported difference between sputtered and evaporated Pt.⁵¹ Importantly, the obtained G_r satisfies the required condition $G_s < G_r$ ^{43,50} which confirms the validity of our estimation.

Conclusions

We present a complete and novel theoretical framework based on the drift-diffusion equations to accurately describe electronic transport in systems with ISOC at non-magnetic metal/insulator interfaces. Within our model, the interface is described by two type of processes: spin losses, parameterized by the interfacial conductances $G_{\parallel/\perp}$, and spin-charge interconversions, quantified by σ_{sc} and σ_{cs} . These parameters are material-specific. The efficiency of the interconversion is quantified by the ratio $\sigma_{sc}/G_{\parallel}$, which coincides with the commonly used Edelstein length λ_{IEE} . The Onsager reciprocity is directly captured by $\sigma_{sc} = \sigma_{cs}$, as demonstrated by comparing our theoretical and experimental results. Our theory is an effective tool for an accurate quantification of spin-charge interconversion phenomena at interfaces, which is of paramount importance in many novel spintronic devices.

Acknowledgement

C.S-F, F.S.B., and I.V.T acknowledge funding by the Spanish Ministerio de Ciencia, Innovación y Universidades (MICINN) (Projects No. FIS2016-79464-P and No. FIS2017-82804-P), by Grupos Consolidados UPV/EHU del Gobierno Vasco (Grant No. IT1249-19). The work of F.S.B. is partially funded by EUs Horizon 2020 research and innovation program under Grant Agreement No. 800923 (SUPERTED). The work at nanoGUNE is supported by Intel Corporation through the Semiconductor Research Corporation under MSR-INTEL TASK 2017-IN-2744 and the “FEINMAN” Intel Science Technology Center, and by the Spanish MICINN under the Maria de Maeztu Units of Excellence Programme (MDM-2016-0618) and under project number MAT2015-65159-R and RTI2018-094861-B-100. V.T.P. acknowledges postdoctoral fellowship support from “Juan de la Cierva–Formacín” program by the Spanish MICINN (grant numbers FJCI-2017-34494). E.S. thanks the Spanish MECD for a PhD fellowship (grant number FPU14/03102).

Supporting Information Available

The following files are available free of charge.

- Additional details on the derivation of the spin-to-charge averaged voltage, Eq. (7), and the renormalized spin diffusion length and node boundary condition for the LSV, Eqs. (8) and (9), respectively; measured temperature dependence of the Cu resistivity and analysis on the temperature dependence of the ISOC parameters in the LSV; brief explanation of the 3D simulation and the relation between the simulation and ISOC parameters; theoretical result for the transverse resistance measured in the multilayer Hall bar, i.e., which leads to Eq. (14). The experimental details of the nanofabrication and measurements of the LSV and multilayer Hall bar devices are also included.

References

- (1) Žutić, I.; Fabian, J.; Das Sarma, S. Spintronics: Fundamentals and applications. *Rev. Mod. Phys.* **2004**, *76*, 323–410.
- (2) Vignale, G. Ten Years of Spin Hall Effect. *Journal of Superconductivity and Novel Magnetism* **2009**, *23*, 3.
- (3) Sinova, J.; Valenzuela, S. O.; Wunderlich, J.; Back, C. H.; Jungwirth, T. Spin Hall effects. *Rev. Mod. Phys.* **2015**, *87*, 1213–1260.
- (4) Valenzuela, S. O.; Tinkham, M. Direct electronic measurement of the spin Hall effect. *Nature* **2006**, *442*, 176–179.
- (5) Kimura, T.; Otani, Y.; Sato, T.; Takahashi, S.; Maekawa, S. Room-Temperature Reversible Spin Hall Effect. *Phys. Rev. Lett.* **2007**, *98*, 156601.
- (6) Aronov, A.; Lyanda-Geller, Y. B. Nuclear electric resonance and orientation of carrier spins by an electric field. *Soviet Journal of Experimental and Theoretical Physics Letters* **1989**, *50*, 431.
- (7) Edelstein, V. M. Spin polarization of conduction electrons induced by electric current in two-dimensional asymmetric electron systems. *Solid State Communications* **1990**, *73*, 233–235.
- (8) Ando, Y.; Shiraishi, M. Spin to charge interconversion phenomena in the interface and surface states. *Journal of the Physical Society of Japan* **2017**, *86*, 011001.
- (9) Soumyanarayanan, A.; Reyren, N.; Fert, A.; Panagopoulos, C. Emergent phenomena induced by spin–orbit coupling at surfaces and interfaces. *Nature* **2016**, *539*, 509–517.
- (10) Miron, I. M.; Garello, K.; Gaudin, G.; Zermatten, P.-J.; Costache, M. V.; Auffret, S.; Bandiera, S.; Rodmacq, B.; Schuhl, A.; Gambardella, P. Perpendicular switching of

- a single ferromagnetic layer induced by in-plane current injection. *Nature* **2011**, *476*, 189–193.
- (11) Liu, L.; Pai, C.-F.; Li, Y.; Tseng, H.; Ralph, D.; Buhrman, R. Spin-torque switching with the giant spin Hall effect of tantalum. *Science* **2012**, *336*, 555–558.
- (12) Safeer, C.; Jué, E.; Lopez, A.; Buda-Prejbeanu, L.; Auffret, S.; Pizzini, S.; Boulle, O.; Miron, I. M.; Gaudin, G. Spin-orbit torque magnetization switching controlled by geometry. *Nature nanotechnology* **2016**, *11*, 143.
- (13) Pham, V. T.; Groen, I.; Manipatruni, S.; Choi, W. Y.; Nikonov, D. E.; Sagasta, E.; Lin, C.-C.; Gosavi, T. A.; Marty, A.; Hueso, L. E.; Young, I. A.; Casanova, F. Spinorbit magnetic state readout in scaled ferromagnetic/heavy metal nanostructures. *Nature Electronics* **2020**, *3*, 309–315.
- (14) Manipatruni, S.; Nikonov, D. E.; Lin, C.-C.; Gosavi, T. A.; Liu, H.; Prasad, B.; Huang, Y.-L.; Bonturim, E.; Ramesh, R.; Young, I. A. Scalable energy-efficient magnetoelectric spin-orbit logic. *Nature* **2019**, *565*, 35–42.
- (15) Karube, S.; Kondou, K.; Otani, Y. Experimental observation of spin-to-charge current conversion at non-magnetic metal/Bi2O3 interfaces. *Applied Physics Express* **2016**, *9*, 033001.
- (16) Kim, J.; Chen, Y.-T.; Karube, S.; Takahashi, S.; Kondou, K.; Tatara, G.; Otani, Y. Evaluation of bulk-interface contributions to Edelstein magnetoresistance at metal/oxide interfaces. *Phys. Rev. B* **2017**, *96*, 140409.
- (17) Nakayama, H.; Kanno, Y.; An, H.; Tashiro, T.; Haku, S.; Nomura, A.; Ando, K. Rashba-Edelstein Magnetoresistance in Metallic Heterostructures. *Phys. Rev. Lett.* **2016**, *117*, 116602.

- (18) Tsai, H.; Karube, S.; Kondou, K.; Yamaguchi, N.; Ishii, F.; Otani, Y. Clear variation of spin splitting by changing electron distribution at non-magnetic metal/Bi₂O₃ interfaces. *Scientific reports* **2018**, *8*, 1–8.
- (19) Rojas-Sánchez, J.-C.; Oyarzún, S.; Fu, Y.; Marty, A.; Vergnaud, C.; Gambarelli, S.; Vila, L.; Jamet, M.; Ohtsubo, Y.; Taleb-Ibrahimi, A.; Le Fèvre, P.; Bertran, F.; Reyren, N.; George, J.-M.; Fert, A. Spin to Charge Conversion at Room Temperature by Spin Pumping into a New Type of Topological Insulator: α -Sn Films. *Phys. Rev. Lett.* **2016**, *116*, 096602.
- (20) Kondou, K.; Yoshimi, R.; Tsukazaki, A.; Fukuma, Y.; Matsuno, J.; Takahashi, K.; Kawasaki, M.; Tokura, Y.; Otani, Y. Fermi-level-dependent charge-to-spin current conversion by Dirac surface states of topological insulators. *Nature Physics* **2016**, *12*, 1027–1031.
- (21) Lesne, E.; Fu, Y.; Oyarzun, S.; Rojas-Sánchez, J.; Vaz, D.; Naganuma, H.; Sicoli, G.; Attané, J.-P.; Jamet, M.; Jacquet, E., et al. Highly efficient and tunable spin-to-charge conversion through Rashba coupling at oxide interfaces. *Nature materials* **2016**, *15*, 1261–1266.
- (22) Vaz, D. C.; Noël, P.; Johansson, A.; Göbel, B.; Bruno, F. Y.; Singh, G.; Mckeown-Walker, S.; Trier, F.; Vicente-Arche, L. M.; Sander, A., et al. Mapping spin–charge conversion to the band structure in a topological oxide two-dimensional electron gas. *Nature materials* **2019**, *18*, 1187–1193.
- (23) Linder, J.; Yokoyama, T. Spin Current in Generic Hybrid Structures due to Interfacial Spin-Orbit Scattering. *Phys. Rev. Lett.* **2011**, *106*, 237201.
- (24) Tokatly, I. V.; Krasovskii, E. E.; Vignale, G. Current-induced spin polarization at the surface of metallic films: A theorem and an *ab initio* calculation. *Phys. Rev. B* **2015**, *91*, 035403.

- (25) Borge, J.; Tokatly, I. V. Ballistic spin transport in the presence of interfaces with strong spin-orbit coupling. *Phys. Rev. B* **2017**, *96*, 115445.
- (26) Borge, J.; Tokatly, I. V. Boundary conditions for spin and charge diffusion in the presence of interfacial spin-orbit coupling. *Phys. Rev. B* **2019**, *99*, 241401.
- (27) Sanz-Fernández, C.; Borge, J.; Tokatly, I. V.; Bergeret, F. S. Nonlocal magnetoelectric effects in diffusive conductors with spatially inhomogeneous spin-orbit coupling. *Phys. Rev. B* **2019**, *100*, 195406.
- (28) Amin, V. P.; Zemen, J.; Stiles, M. D. Interface-Generated Spin Currents. *Phys. Rev. Lett.* **2018**, *121*, 136805.
- (29) Amin, V. P.; Stiles, M. D. Spin transport at interfaces with spin-orbit coupling: Phenomenology. *Phys. Rev. B* **2016**, *94*, 104420.
- (30) Amin, V. P.; Stiles, M. D. Spin transport at interfaces with spin-orbit coupling: Formalism. *Phys. Rev. B* **2016**, *94*, 104419.
- (31) Takahashi, S.; Maekawa, S. Spin injection and detection in magnetic nanostructures. *Phys. Rev. B* **2003**, *67*, 052409.
- (32) Niimi, Y.; Suzuki, H.; Kawanishi, Y.; Omori, Y.; Valet, T.; Fert, A.; Otani, Y. Extrinsic spin Hall effects measured with lateral spin valve structures. *Phys. Rev. B* **2014**, *89*, 054401.
- (33) Isshiki, H.; Muduli, P.; Kim, J.; Kondou, K.; Otani, Y. Experimentally determined correlation between direct and inverse Edelstein effects at Bi₂O₃/Cu interface by means of spin absorption method using lateral spin valve structure. *arXiv preprint arXiv:1901.03095* **2019**,

- (34) Pham, V. T.; Vila, L.; Zahnd, G.; Marty, A.; Savero-Torres, W.; Jamet, M.; Attan, J.-P. Ferromagnetic/Nonmagnetic Nanostructures for the Electrical Measurement of the Spin Hall Effect. *Nano Letters* **2016**, *16*, 6755–6760, PMID: 27712075.
- (35) Kimura, T.; Hamrle, J.; Otani, Y. Estimation of spin-diffusion length from the magnitude of spin-current absorption: Multiterminal ferromagnetic/nonferromagnetic hybrid structures. *Phys. Rev. B* **2005**, *72*, 014461.
- (36) Kimura, T.; Hamrle, J.; Otani, Y.; Tsukagoshi, K.; Aoyagi, Y. Spin-dependent boundary resistance in the lateral spin-valve structure. *Applied Physics Letters* **2004**, *85*, 3501–3503.
- (37) Isasa, M.; Martínez-Velarte, M. C.; Villamor, E.; Magén, C.; Morellón, L.; De Teresa, J. M.; Ibarra, M. R.; Vignale, G.; Chulkov, E. V.; Krasovskii, E. E.; Hueso, L. E.; Casanova, F. Origin of inverse Rashba-Edelstein effect detected at the Cu/Bi interface using lateral spin valves. *Phys. Rev. B* **2016**, *93*, 014420.
- (38) Sagasta, E.; Omori, Y.; Isasa, M.; Otani, Y.; Hueso, L. E.; Casanova, F. Spin diffusion length of Permalloy using spin absorption in lateral spin valves. *Applied Physics Letters* **2017**, *111*, 082407.
- (39) Tsai, H.; Kondou, K.; Otani, Y. Enhanced spin-to-charge current conversion at metal/oxide interfaces by lowering the temperature. *Japanese Journal of Applied Physics* **2019**, *58*, 110907.
- (40) Sánchez, J. R.; Vila, L.; Desfonds, G.; Gambarelli, S.; Attané, J.; De Teresa, J.; Magén, C.; Fert, A. Spin-to-charge conversion using Rashba coupling at the interface between non-magnetic materials. *Nature communications* **2013**, *4*, 1–7.
- (41) Chen, Y.-T.; Takahashi, S.; Nakayama, H.; Althammer, M.; Goennenwein, S. T. B.; Saitoh, E.; Bauer, G. E. W. Theory of spin Hall magnetoresistance. *Phys. Rev. B* **2013**, *87*, 144411.

- (42) Nakayama, H.; Althammer, M.; Chen, Y.-T.; Uchida, K.; Kajiwara, Y.; Kikuchi, D.; Ohtani, T.; Geprägs, S.; Opel, M.; Takahashi, S., et al. Spin Hall magnetoresistance induced by a nonequilibrium proximity effect. *Physical review letters* **2013**, *110*, 206601.
- (43) Zhang, X.-P.; Bergeret, F. S.; Golovach, V. N. Theory of Spin Hall Magnetoresistance from a Microscopic Perspective. *Nano Letters* **2019**, *19*, 6330–6337, PMID: 31378061.
- (44) Brataas, A.; Nazarov, Y. V.; Bauer, G. E. Finite-element theory of transport in ferromagnet–normal metal systems. *Physical Review Letters* **2000**, *84*, 2481.
- (45) Vlietstra, N.; Shan, J.; Castel, V.; Ben Youssef, J.; Bauer, G. E. W.; van Wees, B. J. Exchange magnetic field torques in YIG/Pt bilayers observed by the spin-Hall magnetoresistance. *Applied Physics Letters* **2013**, *103*, 032401.
- (46) Althammer, M. et al. Quantitative study of the spin Hall magnetoresistance in ferromagnetic insulator/normal metal hybrids. *Phys. Rev. B* **2013**, *87*, 224401.
- (47) Kosub, T.; Vlez, S.; Gomez-Perez, J. M.; Hueso, L. E.; Fassbender, J.; Casanova, F.; Makarov, D. Anomalous Hall-like transverse magnetoresistance in Au thin films on Y3Fe5O12. *Applied Physics Letters* **2018**, *113*, 222409.
- (48) Das, K. S.; Dejene, F. K.; van Wees, B. J.; Vera-Marun, I. J. Temperature dependence of the effective spin-mixing conductance probed with lateral non-local spin valves. *Applied Physics Letters* **2019**, *114*, 072405.
- (49) Villamor, E.; Isasa, M.; Vélez, S.; Bedoya-Pinto, A.; Vavassori, P.; Hueso, L. E.; Bergeret, F. S.; Casanova, F. Modulation of pure spin currents with a ferromagnetic insulator. *Phys. Rev. B* **2015**, *91*, 020403.
- (50) Cornelissen, L. J.; Peters, K. J. H.; Bauer, G. E. W.; Duine, R. A.; van Wees, B. J. Magnon spin transport driven by the magnon chemical potential in a magnetic insulator. *Phys. Rev. B* **2016**, *94*, 014412.

- (51) Vlietstra, N.; Shan, J.; Castel, V.; van Wees, B. J.; Ben Youssef, J. Spin-Hall magnetoresistance in platinum on yttrium iron garnet: Dependence on platinum thickness and in-plane/out-of-plane magnetization. *Phys. Rev. B* **2013**, *87*, 184421.

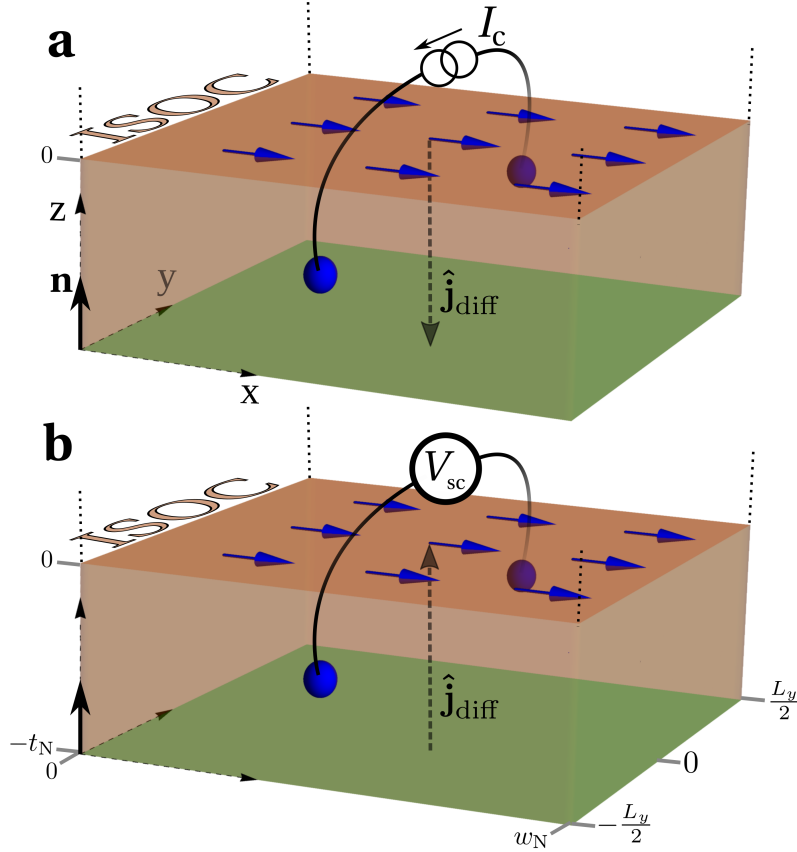


Figure 1: **Sketch of the system under study.** A normal metal, at $z < 0$, is adjacent to a non-magnetic insulator, at $z > 0$. ISOC is finite at the interface with normal vector \mathbf{n} . (a) Charge-to-spin conversion: a charge current I_c induces a spin current density $\hat{\mathbf{j}}_{\text{diff}}$. (b) Spin-to-charge conversion: a spin current density, $\hat{\mathbf{j}}_{\text{diff}}$, induces at the interface a voltage drop perpendicular to the polarization of $\hat{\mathbf{j}}_{\text{diff}}$.

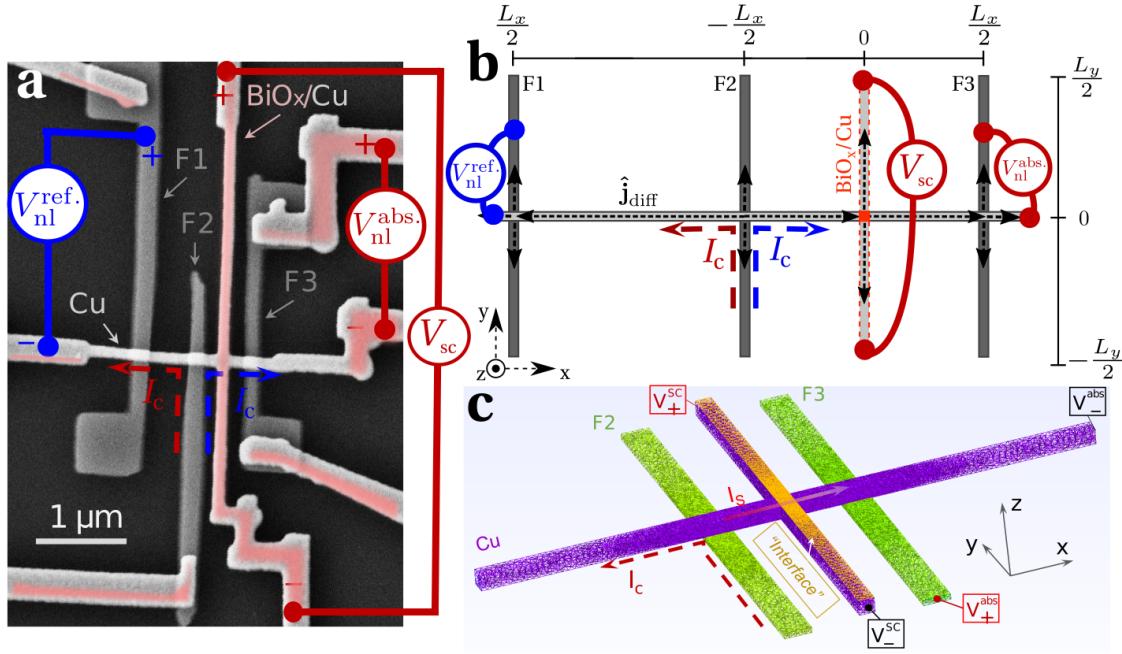


Figure 2: **Lateral spin valve.** (a) SEM image of the two Py/Cu lateral spin valves. The reference LSV uses ferromagnets F1 and F2. Non-local voltage V_{nl}^{ref} is measured (blue circuit). The spin absorption experiment is performed in the LSV between F2 and F3, with a middle Cu wire covered with BiO_x (light red covering). The non-local voltage V_{nl}^{abs} is measured (red circuit). In both cases the external magnetic field is applied along the y axis. The spin to charge conversion is detected by measurement of the transverse voltage V_{sc} after injection of a current from F2 (red circuit). In this case the external magnetic field is applied along the x axis. (b) Effective one-dimensional model of the device. (c) Geometry and mesh of the 3D finite element method model used for simulating the spin absorption and spin-to-charge conversion. The BiO_x/Cu interface is simulated as a thin layer (yellow) on top of the transverse Cu wire (purple).

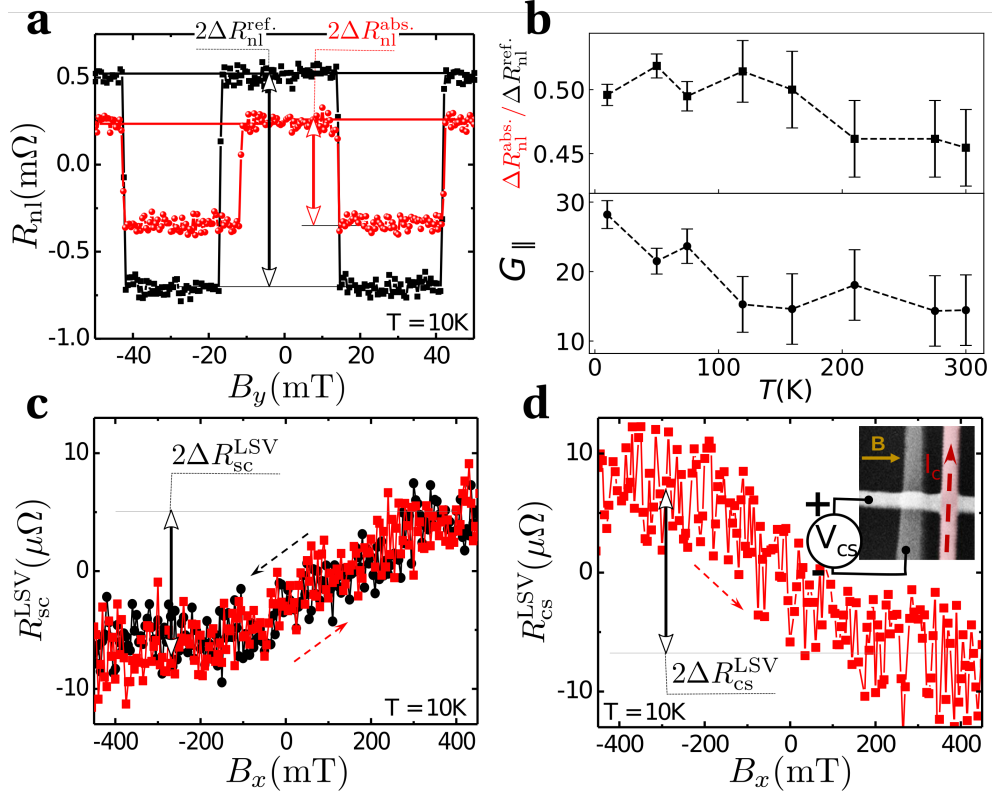


Figure 3: **LSV experimental results.** (a) Non-local resistance as a function of B_y (trace and retrace) measured at $I_c = 70\mu\text{A}$ and 10 K for the reference LSV (black squares) and the LSV with the middle BiO_x/Cu wire (red circles). From this measurement, we extract $\Delta R_{nl}^{\text{ref.}}$ and $\Delta R_{nl}^{\text{abs.}}$. (b) Upper panel: the spin absorption ratio ($\Delta R_{nl}^{\text{abs.}} / \Delta R_{nl}^{\text{ref.}}$) as a function of temperature; lower panel, the corresponding interfacial spin-loss conductance in units of $(\Omega^{-1}\mu\text{m}^{-2})$ as a function of the temperature, calculated from Eq. (11). (c) Non-local resistance as a function of B_x (trace and retrace) measured at $I_c = 70\mu\text{A}$ and 10 K. Each curve is an average of 7 sweeps. The spin-to-charge conversion signal ($2\Delta R_{sc}^{\text{LSV}}$) is extracted. (d) Non-local resistance as a function of B_x (trace only) measured at $I_c = 150\mu\text{A}$ and 10 K using the configuration of the inset, which is reciprocal to the one of panel (c). From this measurement we extract the charge-to-spin conversion signal ($2\Delta R_{cs}^{\text{LSV}}$). The curve is an average of 4 sweeps.

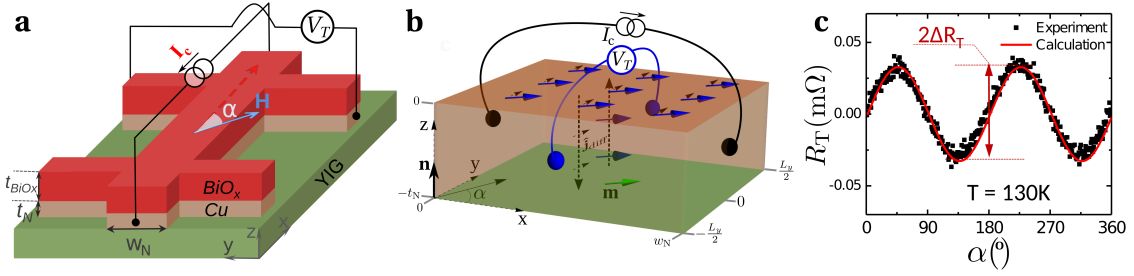


Figure 4: **Spin magnetoresistance in multilayer device.** (a) Measurement configuration of the TADMR in BiO_x/Cu Hall-cross device on YIG. A charge current I_c is applied along the x direction. The external H-field (100 mT) is applied in-plane the YIG substrate, x - y plane, to drive the magnetisation of YIG. A voltmeter is applied to probe the transverse potential change V_T under open circuit conditions. α is the angle between the applied current vector (red dashed arrow) and the applied field (blue solid arrow) in the x - y plane. (b) Sketch of the double spin-charge interconversion at the BiO_x/Cu interface with ISOC. First, charge current I_c injection induces a bulk y -polarized spin current density flowing towards the Cu/YIG interface, where it is back-reflected with mixed x and y polarizations. Secondly, the x -polarized contribution to the spin ECP at the ISOC interface, generates a voltage drop along the y direction. (c) TADMR (R_T) as a function of α . R_T is the value of the measured transverse voltage divided by the applied current I_c (black squares). Solid curve corresponds to $R_T = 0.03 \sin(2\alpha)$.